CEAS-GNC-2022-031

CEAS EuroGNC 2022
"Conference on Guidance, Navigation and Control"
3-5 May 2022 @ Technische Universität Berlin, Germany

Energy optimal flight path planing for unmanned aerial vehicle in urban environments

Hannes Rienecker Dipl.-Ing., Technische Universität Dresden, Chair of Flight Mechanics and Control, 01062, Dresden, Germany. hannes.rienecker@tu-dresden.de

Veit Hildebrand Dr.-Ing., Technische Universität Dresden, Chair of Flight Mechanics and Control, 01062, Dresden, Germany. veit.hildebrand@tu-dresden.de

Harald Pfifer Prof. Dr.-Ing., Technische Universität Dresden, Chair of Flight Mechanics and Control, 01062, Dresden, Germany. harald.pfifer@tu-dresden.de

ABSTRACT

A general approach is presented to compute energy optimal flight paths for unmanned aerial vehicle (UAV) in urban environments. In order to minimize the energy consumption, the flight path is optimized by exploiting local wind phenomena, i.e., upwind and tailwind areas from the airflow around buildings. The approach is demonstrated on a delivery UAV benchmark scenario. As urban environment the so called VDI City Model is chosen. A realistic wind field of the VDI model is generated using the Large Eddy Simulation tool PALM. The calculated wind field is validated with existing wind tunnel measurements from literature. For the flight path planning a novel cost function is proposed that minimizes energy consumption while assuming constant altitude. The A-Star-Algorithm is used to optimize the trajectories in the benchmark. Finally, the results of the energy optimal path planning is compared to shortest way trajectories for four different scenarios. It is shown that energy can be saved while flying in a city by using knowledge of the current wind field.

Keywords: Flight path optimization; Unmanned aerial vehicle; Unmanned aerial system

1 Introduction

Progressive urbanisation requires new, environmentally friendly and efficient mobility concepts. Electrically powered unmanned aerial vehicles (UAV) offer great potential for tackling last-mile logistics [1]. On the one hand, this technology offers benefits such as reducing urban traffic and drastically shortening delivery times, especially for remote locations. On the other hand, energy consumption needs to be carefully considered as these UAS have a lower payload compared to conventional delivery systems [2]. Hence, in order to fully take advantage of airborne delivery systems novel technologies for increasing the energy efficiency of such systems are required. Optimization based approaches for finding energy optimal flight trajectories could lead to a significant power reduction, closing the efficiency gap between airborne and ground-based delivery systems. Specifically, for light-weighted delivery UAS, local wind conditions play an important role in the power consumption.

This paper contributes a benchmark study on potential energy savings by optimizing the flight path of a typical delivery mission using the knowledge of the wind field in an urban environment. The chosen urban setup is the so-called VDI city model taken from [3]. It was chosen for its relative simplicity and

the availability of experimental measurements of its wind field in wind tunnels. Within the city model a typical delivery scenario, i.e., flying from a pick-up point to a drop-off point, is studied. Under different wind conditions energy optimal flight paths are computed and compared to conventional shortest path trajectories. A detailed description of the problem setup is presented in Section 2.

To be a representative benchmark study, a qualitative realistic wind field for the VDI model is necessary. Various methods ranging from simple statistical methods to complex approximative solutions of the atmospheric boundary layer equations exist in literature. For a good overview, the reader is referred to [4]. In this paper the model PALM (Parallelized Large-Eddy Simulation Model, [5]) is used to prognose the wind field. It is a CFD (Computational Fluid Dynamics) simulation, or to be more precise a LES (Large Eddy Simulation).

The ensuring of an energy-optimal flight through different wind conditions is a classical route optimization problem. There are various methods to find an optimal route:

- Branch-and-Bound [6],
- Evolutionary computing, e.g. [7],
- Multiple-agent-systems [8],
- Neural network [9],
- Experience Optimization.

Altogether have the same target to minimize a cost function. Modern airline trajectory optimizations [10] uses the A-star-algorithm, an adaption of the Dijsktra-algorithm. This Branch-and-Bound method has advantages of allowing three dimensional path finding [10] and computation performance efficiency [11]. In [10] horizontal flight paths have been optimized with respect to minimum fuel flow considering lateral impacts (like wind speed and wind direction). In contrast vertical flight path optimization was done therein by a flight performance model and an iterative connection of vertical and lateral movement reaching to one of the best trajectory. Tasks in UAV Flight path planning and optimizing are actual constrained to find one of the shortest trajectory in scenarios with restricted air space [12], agricultural applications such as fertilizers and pesticide spray in crop fields just on stressed regions [13] and military objectives like avoiding enemy radar sites [14].

2 Problem Formulation

Consider a typical scenario of a future logistic UAV on a package delivery mission in an urban environment. The UAV is similar in size and characteristics to a Wingcopter 198 delivery UAV. It is a fully electric fixed wing aircraft with a wing span of 1.98 m and a maximum take-off weight of 25 kg. Best performance cruise speed is 28 m/s, where a glide ratio of 20 is assumed.

The urban environment that was chosen for the present study is an existing, fictional city model from literature [3]. A major advantage of using this city model is the availability of experimental data from several wind tunnels in Germany. The model consists of an arrangement of five different shaped buildings with two different building heights, scaled with the factor 75, as illustrated in Fig. 1 in a wind tunnel setup. One high building has a height of 60 m, or scaled 800 mm respectively as wind tunnel model, and is lying central in the scenario. The four buildings around it have a height of 30 m, or scaled 400 mm respectively. As shown in the figure, the city section is characterized by relatively large and tall buildings. Due to the size of the buildings, their impact on the flow field in the city area is significant. This makes it ideal as a benchmark scenario for showcasing that exploiting local wind effects in urban environments can reduce the energy consumption during a delivery mission.

In the present paper, four distinct scenarios are studied for the considered logistic UAV in the urban benchmark model. These scenarios are depicted in Fig. 2. The scenarios have a common start and end point for the delivery task, indicated by "start" and "end" in the figure. They are 168 m apart from each

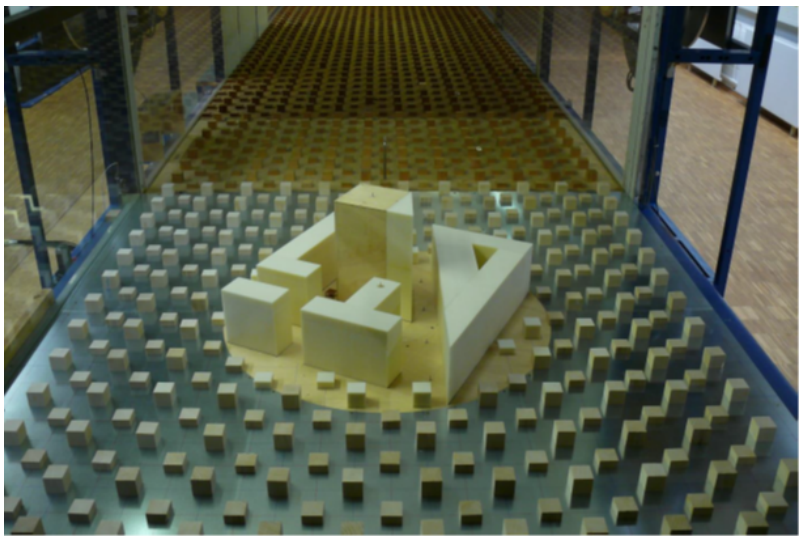

Fig. 1 Urban city model in wind tunnel experiment [3]

other. In each scenario the goal is to minimize the energy consumption of the UAV by using local flow effects to its advantage. The aircraft is always assumed to fly at a constant true airspeed corresponding to its best-performance cruise speed. For each scenario a constant altitude is assumed which reflects the likelihood of having restricted corridors for air delivery in cities. In three simulation scenarios the flight height is 32.5 m, which is shortly above most of the roofs. The wind direction varies in those scenarios, while the wind speed is constant at 0.28 m/s, in accordance with existing wind tunnel test data. In the fourth simulation the flight height is just below the lower building roofs at 25 m and has one wind direction with a wind speed of 2.8 m/s. The true air speed of the UAV is always constant at best-performance cruise speed.

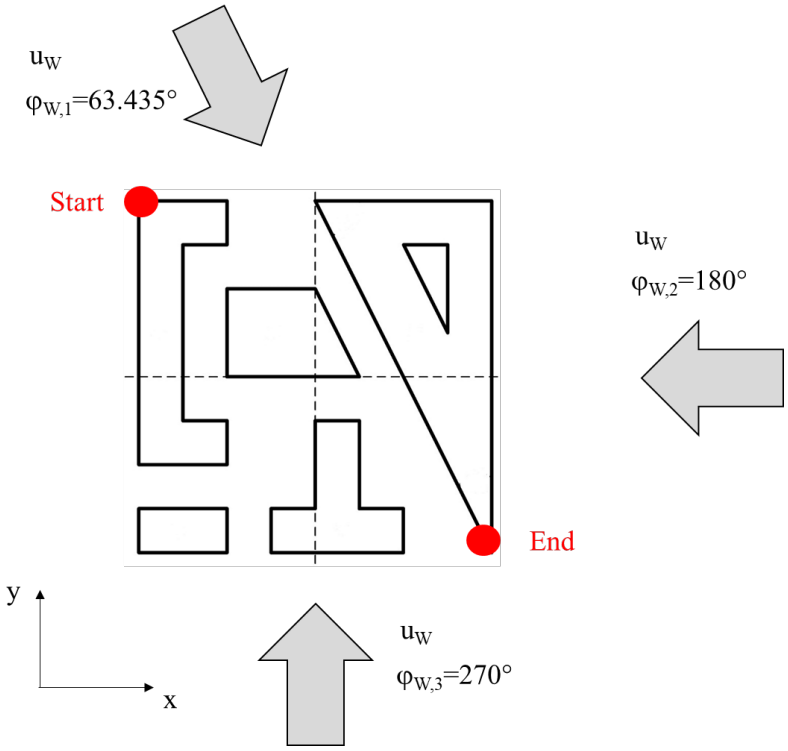

Fig. 2 Test scenario with 3 wind directions, as well as starting and ending point, 168 m apart from each other

3 Wind Field Prediction using LES

This section gives a brief introduction to the PALM model system which is used in the present paper to obtain a realistic wind field within an urban environment for the following flight path optimization. PALM[1] was developed by University of Hannover as a tool to simulate urban climate and its boundary layer [5]. It has been validated for flow around solid obstacles [15, 16] and used in various real urban environments [15–18]. A detailed description of PALM and its capabilities can be found in [5]. In short, PALM calculates the non-hydrostatic, filtered, incompressible Navier-Stokes equations in Boussinesq-approximated form. Furthermore, the subgrid-scale turbulent kinetic energy (SGS-TKE) is solved.

In a first step, the topography of the VDI city model was recreated full-scaled in PALM. For the modeling, PALM uses equidistant horizontal grid spacings. Each grid volume can be either air or solid as a building. Hence oblique walls of buildings must be handled specially. If more than half of the volume is geometric inside of a building, the whole volume will be set as a building. To catch all flow effects around the buildings, an obstacle-free area in the upstream and in the downstream of the city model was placed in the geometry model. Sensitivity studies were conducted to estimate the overall area of the computational model. An upstream area of 150 m in front of and an downstream area of 630 m behind the buildings enable the formation of upstream blocking effect and wake. The grid size for all experiments was set to $\Delta_{x,y,z} = 2.5\,\mathrm{m}$. This size offered the best trade-off between computational time and accurate resolution of flow effects. The same setup was used for the different test cases described in Section 2 with the only difference being a rotation of the building area to implement the different wind directions. The setup of the topography for the scenarios is depicted in Fig. 3.

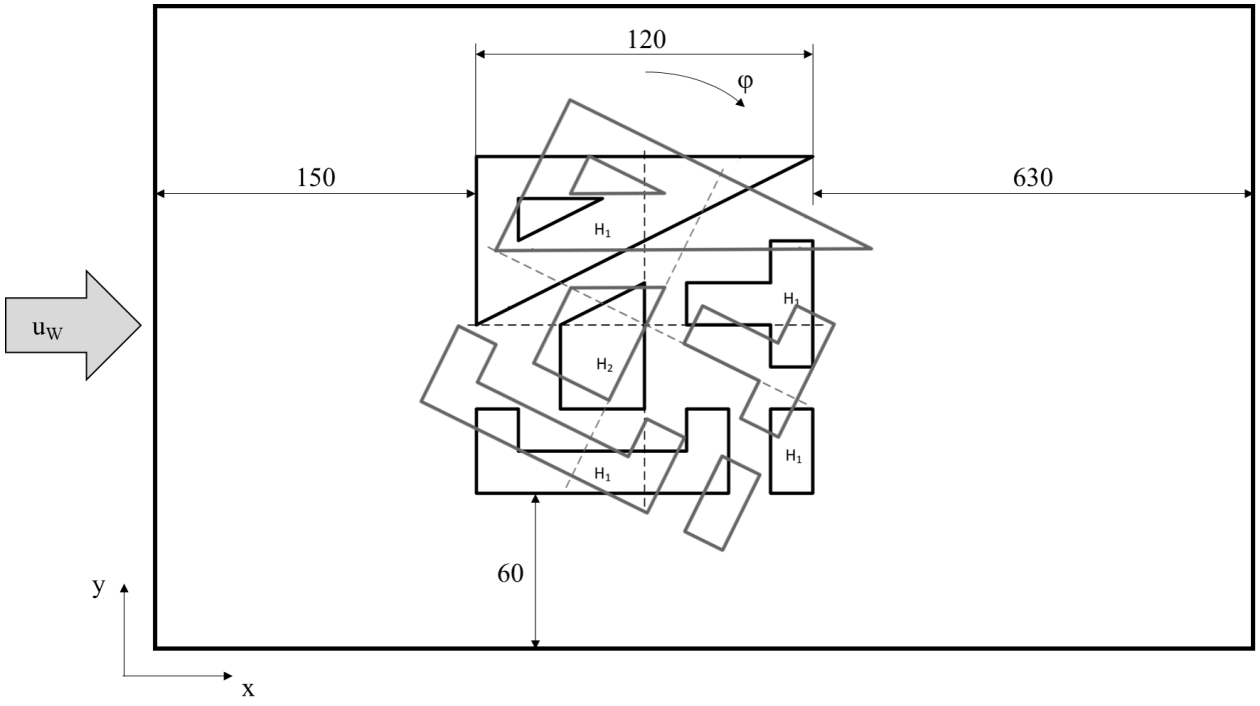

Fig. 3 Test szenario for LES simulation with up- and downstream area

PALM calculates the velocity components u, v, w in the *Arakawa C-grid* [19]. This means that each values for u, v and w do not refer to the same grid point, but to the appropriate side face of the volume mesh. The output data of the wind field calculation in *Arakawa C-grid* is converted into velocity point data. Each knot of grid volume becomes a point. At the transforming process all velocity components of the side faces, which connect to the point, are averaged to obtain the velocity component of the point.

[1] https://palm.muk.uni-hannover.de/

In order to validate the setup of the scenarios in PALM, a comparison study with results from a wind tunnel experiment is presented. The wind tunnel data is taken from [3] and was conducted at TU Dresden. The setup of the wind tunnel experiment is depicted in Fig. 1 The wind direction in the wind tunnel experiment was 63.435°. As shown in Fig. 4, 13 measurement points in 2 m height above ground were used and 2 additional measurement points at the roof level. A hot wire anemometer measured the wind speed at each point.

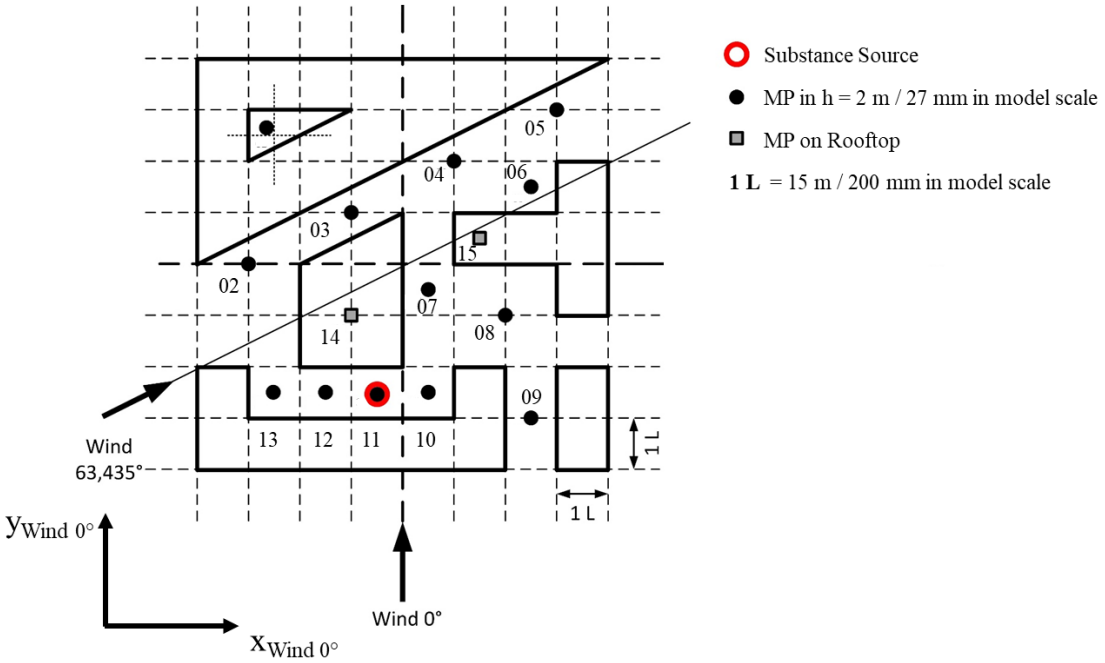

Fig. 4 Measuring points of wind tunnel model

For the validation calculation, the settings shown in Tab. 1 are used for PALM. Before the data is compared to the wind tunnel results, it has to be ensured that the LES is fully developed. In Fig. 5 one can see that subgrid-scale momentum flux $w''u''$ is one order of magnitude smaller than the resolved-scale counterpart w^*u^* after two hours of calculation time. From this it can be concluded that the grid spacing is sufficiently small according to [20]. Furthermore timeseries of kinetic energy E, turbulent kinetic energy E^* and the maximum of velocity components show no trends anymore after 15 100 s ($\approx$ 4 hours) of simulation time, so the simulation was converging.

First, the inflow averaged wind profiles were compared. Fig. 6 shows both, wind tunnel experiment and LES simulation, transformed to 1:1-scale of simulation and relative to u_{ref}, the velocity u in the height of $z = 30$ m. They behave in a good consistency in the range of the building height. The variations above 50 m are outside the used range and therefore not of interest.

The measuring points of the wind tunnel experiment, as depicted in Fig. 4, have some discrepancies. Tab. 2 shows the measured wind speed u_{Exp} in a height of ca. 2 m, compared to the wind speed in LES simulation in the height of 2.5 m. Because of grid spacing the comparison is not on the same level. There is a good consistency for the first point in flow field, Pt. 2. The following measuring points are heavily influenced by the wall impact and it is challenging to achieve good results in almost ground level with turbulent flow. Moreover the inflow velocity of 0.28 m/s is relatively low. Numerical errors cannot be excluded. Furthermore the measuring points in LES are on top of the bottom layer. PALM uses a constant flux layer there, which has influences on volume-averaged velocity variables. According to [21] this leads to underestimation of the surface fluxes in simulation as it can be seen predominantly in Tab. 2.

Table 1 Used settings in the LES model PALM

Setting	Set in Computation
Turbulence closure	1.5-order according to Deardorff
Pertubation Pressure Solver	FFT with temperton-algorithm routines
Momentum advection	Wicker-Skamarock-Scheme 5th order
Scalar advection	Wicker-Skamarock-Scheme 5th order
Boundary Conditions	Horizontal: cyclic boundary conditions
	Volume Flow Conservation at right and north boundary
	Bottom and Building walls: Constant flux layer following Monin-Obukhov similarity theory
	Top: free-slip conditions
Instream	bulk velocity u_b with 1D wind profile for initialization
Discretization (space)	Finite differences (Unchangeable)
Grid Size nx	360 (corresponds to 900 m)
ny	96 (corresponds to 240 m)
nz	40 (corresponds to 100 m)
Discretization (time)	Runge-Kutta-3
End Time	14400 s
Averaging Output Time	3600 s
Coriolis force	Switched Off
External forcing and nesting	Switched Off
Ocean option and coupling to atmosphere	Switched Off
Embedded models	Switched Off

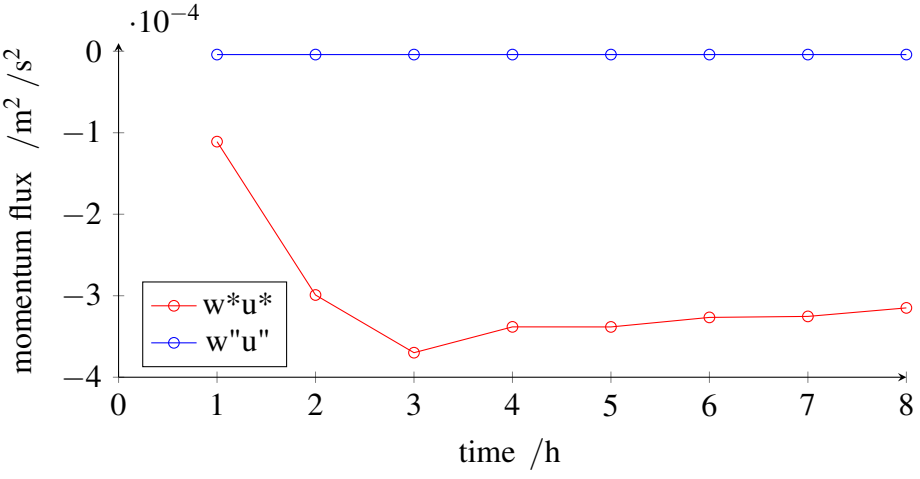

Fig. 5 Subgrid-scale momentum flux $w''u''$ and resolved-scale counterpart w^*u^*, for each mean value over the height

The focus of this paper was not to find a precise numeric solution, but to get reasonable values of air flow in urban area with respect to computation time. The simulation is sufficient enough to conclude that a realistic flow in urban area is available.

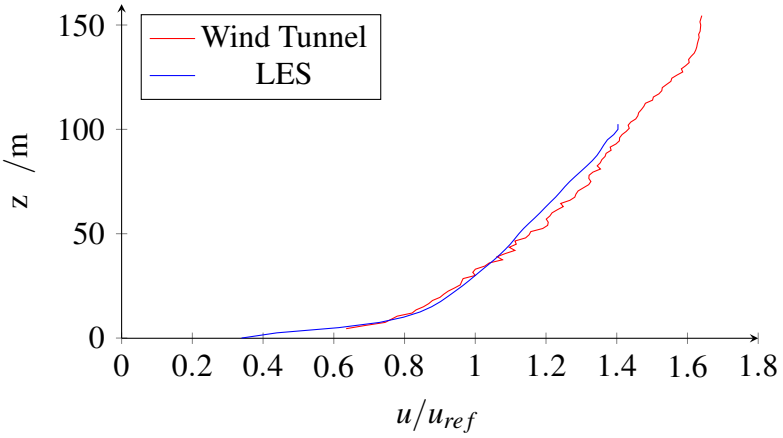

Fig. 6 Comparison between wind profile of wind tunnel experiment and LES simulation

Table 2 Comparison between measuring points of wind tunnel experiment and LES simulation with $\Delta = |u_{Exp} - u_{LES}|/u_\infty$

MP	u_{Exp}	$u_{LES,h=2.5m}$ in m/s	Δ in %
2	0.106	0.101	2.2
3	0.131	0.183	23.5
4	0.128	0.161	15.1
5	0.120	0.129	4.0
6	0.024	-0.011	15.9
7	0.083	-0.014	44.3
8	0.083	0.014	31.6
9	0.058	0.008	22.6
10	0.076	0.111	16.0
12	0.089	-0.066	70.7
13	0.108	0.092	7.4

4 Trajectory Optimization

The objective of the flight path planning is to minimize a cost function J,

$$J = \int_{s_0}^{s_f} A(X,s)\,\mathrm{ds}, \tag{1}$$

where X is the position vector of the aircraft, s_f the arrival point and $A(X,s)$ the quantity to be minimized at each step. To minimize the distance, for instance, $A(X,s)$ is set to $A(X,s) = 1$. In general, this is a complex optimization problem that is usually solved over a discrete grid instead of the continuous integral. Multiple solver exist in literature to minimize Eq. (1), e.g., the in this paper used Branch-and-Bound algorithm [6] or evolutionary computing based ones [7].

4.1 Branch and Bound Algorithm

The *A-Star-Algorithm* is an adaption of the Dijsktra-algorithm [11]. The used model is a pathfinding from starting to ending point in respect of its cost. Different paths are identified by the waypoints or knots of the wind field grid of LES, except of the knots, which where inside building or part of a wall. The algorithm combines two advantageous information. First the exact cost of the path from the starting point

to any knot n and second, the heuristic estimated cost from knot n to the ending point. The algorithm balances both costs as it moves from the starting point to the goal per knot. Each time through the main loop, it examines the knot n that has the lowest total cost. The algorithm is ending the checking for a path if another path with lower cost was found before. Hence, the algorithm checks from staring point all possible paths, but breaks if they were considered too bad. This approach leads to savings in computation time, because not all possible paths were computed.

4.2 Cost Function

The optimization problem in the present paper is to minimize the energy consumption of the propulsion system for the UAV for a fixed start and end point and a constant altitude, see Section 2 for the detailed problem. All flight mechanical assumptions are derived from corresponding standard literature, e.g. [22]. The constant altitude is motivated by the reasonable real life requirement that the UAV has to fly within a prescribed corridor. In order to achieve an optimal flight trajectory a new cost function is proposed which is detailed in this section. First, the generic flight path cost function (2) is defined as an integral over the flight path s and then discretized in sequentially flown through grid points until ending point N.

$$J = \int_{s_0}^{s_e} A(s)\,\mathrm{ds} = \sum_{i=0}^{N} A_i\,\Delta s_i. \tag{2}$$

For simplification, the energy consumption of the propulsion system is assumed to be proportional to the thrust force multiplied with the path covered by the UAV. Further, for the UAV in steady cruise flight it is assumed that the thrust force is equal to the aerodynamic drag force D. Using this assumption, the energy consumption between two points of the discretized flight path E_i is given by

$$E_i = D \cdot \Delta s_i = D \cdot u_{E,TAS} \cdot \Delta t_i \tag{3}$$

where $u_{E,TAS}$ is the true airspeed (TAS) and Δt_i is the time required to cover the distance between two grid points Δs_i. Defining $u^*_{E,i}$ as the ground speed at the i-th grid point, the time it takes to cover Δs_i is given by

$$\Delta t_i = \frac{\Delta s_i}{u^*_{E,i}}\,. \tag{4}$$

With respect to headwind $u_{W,i}$ and the crosswind component $v_{W,i}$, these components decrease the ground speed u^*_E to:

$$u^*_{E,i} = \sqrt{(u_{E,TAS} - u_{W,i})^2 - v^2_{W,i}}\,. \tag{5}$$

Upwind components are considered as follows: There is no change in flight height due to it. The Nose of UAV pitches downwards to hold the flight level. Hence, the upwind $w_{W,i}$ leads to a decrease of the flight path angle γ_i:

$$\sin(\gamma_i) = \frac{w_{W,i}}{u^*_{E,i}}\,. \tag{6}$$

This change of flight path angle leads to less thrust due to the balances of flight mechanic forces, because the weight force supports the force in flight direction. Considering Eq. (3), where thrust equals drag, results this support of gravity in a perceived decrease of drag to:

$$D_i = D_0 - \sin(\gamma_i) \cdot mg \tag{7}$$

with D_0 as drag force in normal horizontal flight condition and mg the weight force. Hence, using Eq. (3), (4), (5) and (7) yields the following equation for the energy consumption between two knots:

$$E_i = \frac{\Delta s_i}{\sqrt{(u_{E,TAS} - u_{W,i})^2 - v_{W,i}^2}} \cdot (D_0 - \sin(\gamma_i) \cdot mg) \cdot u_{E,TAS}\,. \tag{8}$$

The definition of D_0 is set by the gliding ratio Υ:

$$D_0 = \frac{L}{\Upsilon} = \frac{mg}{\Upsilon} \tag{9}$$

with L as lift force equal to the weight force and the glide ratio Υ of the fixed-wing UAV. Using Eq. (8) and (9), the cost function for the minimization of the energy consumption can be written in the following way:

$$E = \sum_{i=0}^{N} \frac{\Delta s_i}{\sqrt{(u_{E,TAS} - u_{W,i})^2 - v_{W,i}^2}} \cdot (D_0 - \sin(\gamma_i) \cdot mg) \cdot u_{E,TAS}\,. \tag{10}$$

5 Results of Trajectory Optimization

In this section the results of the flight path optimization using the cost function proposed in the previous section are presented. Overall, 4 different scenarios are tested according to the problem formulation in Section 2. Specifically, these are three scenarios at a wind speed of 0.28 m/s with 63.435°, 180° and 270° wind direction respectively, and one scenario at 2.8 m/s wind speed and 63.435° wind direction. For each scenario two different optimal trajectories are computed. The first one is based on the energy optimal cost function of Eq. (10). The second one is a simple shortest path optimization as described in Eq. (2). The optimization itself is in each case performed by the same a-star-algorithm. The grid resolution of trajectory optimization is the same as in LES wind field prediction with $\Delta_{x,y} = 2.5$ m.

Tab. 3 - 5 show the results for the low wind speed, i.e. 0.28 m/s, scenarios. Due to the relative low wind speed with respect to the flight speed of 28 m/s, no significant differences between energy and path optimal trajectories can be expected. Still even at almost no wind, using knowledge of the wind field allows energy savings between 0.3-2.0%. It shall be emphasized that the flight path is not becoming significantly longer or even the same as in Tab. 3. The shortest path optimization having no knowledge of the current wind field, simply cannot differentiate between energy differences of paths of the same length. Hence, even with the same flight distance the energy optimization can achieve an energy reduction. Note that the difference of shortest way in 63.435°-scenario to the other ones is due to resolution of rotated grid, see Fig. 3.

Table 3 Comparison between shortest-way-optimization and energy-optimization, wind speed 0.28 m/s, direction 63.435°.

Cost Function	flight track in m	Difference in %	Energy Consumption in J	Difference in %
Shortest way	181.7		2218.3	
Energy	181.7	±0	2185.3	**-1.5**

An example of the actual flight paths is given in Fig. 7, where orange is the shortest path and blue the lowest energy consumption. Note that most of the energy savings actually come from exploiting regions of upwind and not tailwinds. This becomes clear when looking at the upwind along the trajectories, see Fig. 8. The energy optimized trajectory is flying through much larger upwind fields than the shortest way. If one look at Eq. (8), it can be seen that small differences of upwind have a greater impact on

Table 4 Comparison between shortest-way-optimization and energy-optimization, wind speed 0.28 m/s, direction 180°. Difference of shortest way to 63.435°-scenario due to resolution of rotated grid, see Fig. 3.

Cost Function	flight track in m	Difference in %	Energy Consumption in J	Difference in %
Shortest way	186.2		2252.1	
Energy	186.2	±0	2245.5	**-0.3**

Table 5 Comparison between shortest-way-optimization and energy-optimization, wind speed 0.28 m/s, direction 270°

Cost Function	flight track in m	Difference in %	Energy Consumption in J	Difference in %
Shortest way	186.2		2268.5	
Energy	187.7	**+0.8**	2224.1	**-2.0**

energy consumption than small ones of tailwinds. Furthermore, it must be said that no path smoothing is considered. The flight path is just allowed from grid point to adjacent grid point. Hence there are some kinks where a direct line is expected.

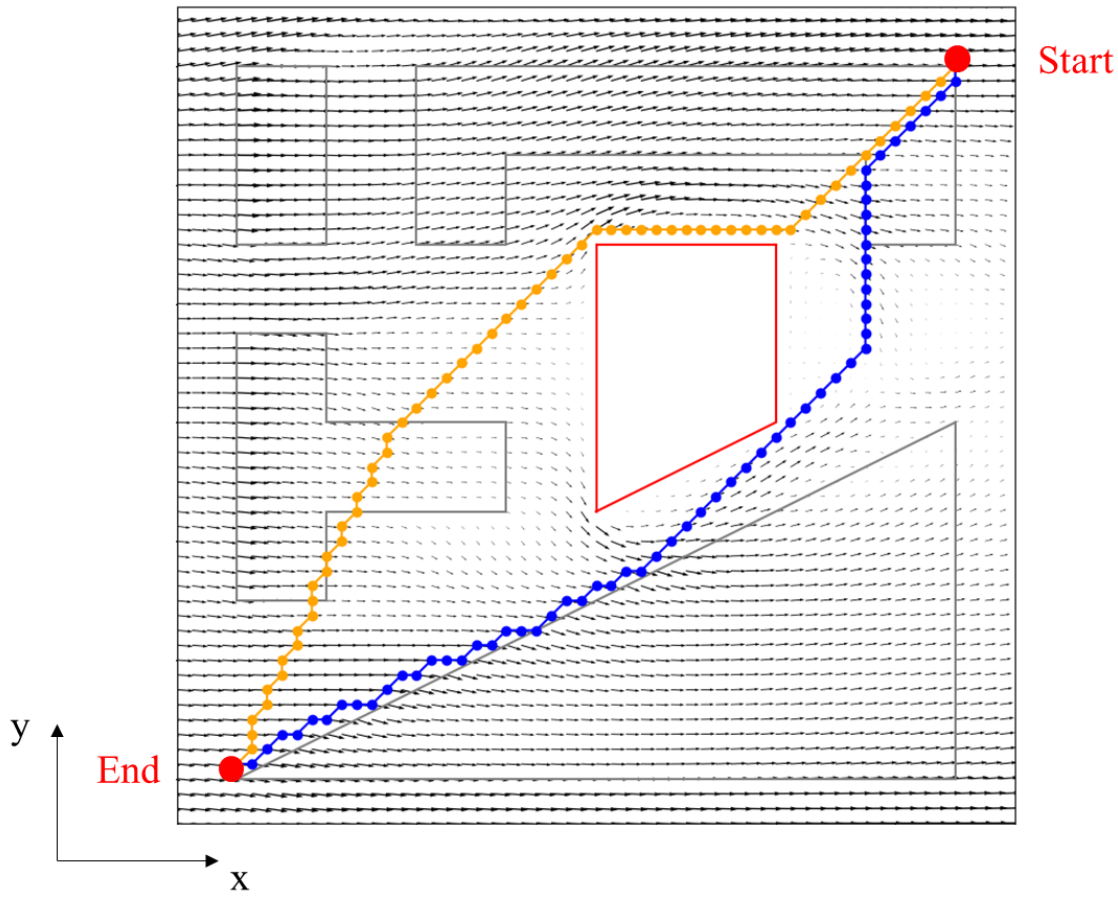

Fig. 7 Horizontal wind velocity field, flight path of shortest-way-optimized (orange) and energy-optimized (blue) flight at wind speed 0.28 m/s, direction 270°

Finally, the results of the higher wind speed of 2.8 m/s are presented in Tab. 6. As expected, the higher wind speed offers more advantages for the energy optimal flight path. In this scenario, a energy reduction of 31.4% can be achieved.

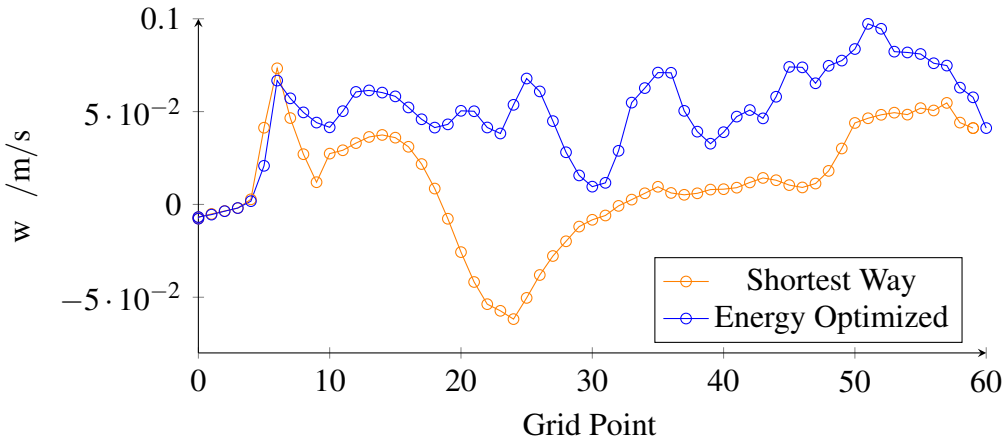

Fig. 8 Vertical wind velocity component w on flight path of shortest-way-optimized (orange) and energy-optimized (blue) flight at wind speed 0.28 m/s, direction 270°

Table 6 Comparison between shortest-way-optimization and energy-optimization, wind speed 2.8 m/s, direction 63.435°

Cost Function	flight track in m	Difference in %	Energy Consumption in J	Difference in %
Shortest way	153.0		1930.6	
Energy	159.2	**+3.9**	1469.2	**-31.4**

A flight path comparison for this scenario is presented in Fig. 9 with the shortest path in orange and the lowest energy consumption in blue. Again, while superficially it looks like the shortest path is making good use of tailwind, it is actual the efficient exploitation of upwind that allows the large energy savings of the blue trajectory.

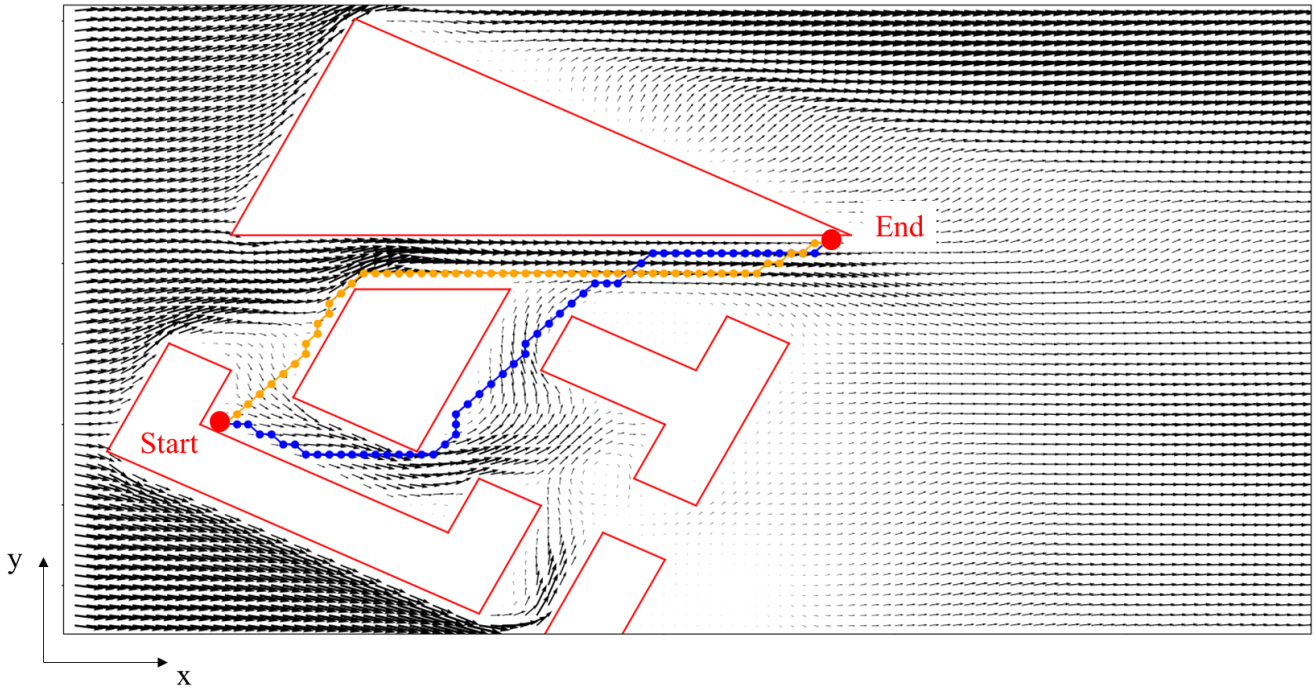

Fig. 9 Horizontal wind velocity field, flight path of shortest-way-optimized (orange) and energy-optimized (blue) flight at wind speed 2.8 m/s, direction 63.435°

6 Conclusion

In this paper an approach to optimize the horizontal flight trajectory of a delivery UAV in respect of energy consumption was presented. The wind field behind this approach was obtained by a LES simulation. It was shown, that the simulation grid was sufficient. The prognosis of a wind field in urban area via LES is realistic. The main result is, that it is always beneficial to optimize the flight path even at close to zero wind speed. If the wind speed is moderate, the influence will be significant.
As an outlook more attention will be put in the future on the weather input data with respect to a real flight application. Combined with real measurement from weather stations and onboard measurements in UAV a realistic wind field will allow an better assessment of the potential of energy optimal flight path planing for UAVs in urban environments.

References

[1] Tom Plümmer. Die fliegenden Helfer – sichere und schnelle Hilfe durch Wingcopter. In *Smart City – Made in Germany*, pages 613–617. Springer Fachmedien Wiesbaden, 2020. DOI: 10.1007/978-3-658-27232-6_64.

[2] Thomas Kirschstein. Comparison of energy demands of drone-based and ground-based parcel delivery services. *Transportation Research Part D: Transport and Environment, Vol. 78*, 78:102209, jan 2020. DOI: 10.1016/j.trd.2019.102209.

[3] VDI-Richtlinie 3783 (Gründruck). Umweltmeteorologie - Physikalische Modellierung von Strömungs- und Ausbreitungsvorgängen in der atmosphärischen Grenzschicht - Windkanalanwendungen, 2021.

[4] Philipp Oettershagen, Benjamin Muller, Florian Achermann, and Roland Siegwart. Real-time 3d wind field prediction onboard UAVs for safe flight in complex terrain. In *2019 IEEE Aerospace Conference*. IEEE, mar 2019. DOI: 10.1109/aero.2019.8742160.

[5] B. Maronga, M. Gryschka, R. Heinze, F. Hoffmann, F. Kanani-Sühring, M. Keck, K. Ketelsen, M. O. Letzel, M. Sühring, and S. Raasch. The parallelized large-eddy simulation model (PALM) version 4.0 for atmospheric and oceanic flows: model formulation, recent developments, and future perspectives. *Geoscientific Model Development*, 8(8):2515–2551, aug 2015. DOI: 10.5194/gmd-8-2515-2015.

[6] A. H. Land and A. G. Doig. An automatic method of solving discrete programming problems. *Econometrica*, 28(3):497, jul 1960. DOI: 10.2307/1910129.

[7] José Tarcísio Franco de Camargo, Eliana Anunciato Franco de Camargo, Estéfano Vizconde Veraszto, Gilmar Barreto, Jorge Cândido, and Patricia Aparecida Zibordi Aceti. Route planning by evolutionary computing: an approach based on genetic algorithms. *Procedia Computer Science*, 149:71–79, 2019. DOI: 10.1016/j.procs.2019.01.109.

[8] Sumana Biswas, Sreenatha G. Anavatti, and Matthew A. Garratt. Particle swarm optimization based cooperative task assignment and path planning for multi-agent system. In *2017 IEEE Symposium Series on Computational Intelligence (SSCI)*. IEEE, nov 2017. DOI: 10.1109/ssci.2017.8280872.

[9] Jinglun Yu, Yuancheng Su, and Yifan Liao. The path planning of mobile robot by neural networks and hierarchical reinforcement learning. *Frontiers in Neurorobotics*, 14, oct 2020. DOI: 10.3389/fnbot.2020.00063.

[10] Judith Rosenow, Martin Lindner, and Hartmut Fricke. Assessment of air traffic networks considering multicriteria targets in network and trajectory optimization. In *Deutscher Luft- und Raumfahrtkongress 2015*, 09 2015.

[11] Peter Hart, Nils Nilsson, and Bertram Raphael. A formal basis for the heuristic determination of minimum cost paths. *IEEE Transactions on Systems Science and Cybernetics*, 4(2):100–107, 1968. DOI: 10.1109/tssc.1968.300136.

[12] Luitpold Babel. Flight path planning for unmanned aerial vehicles with landmark-based visual navigation. *Robotics and Autonomous Systems*, 62(2):142–150, feb 2014. DOI: 10.1016/j.robot.2013.11.004.

[13] Kshitij Srivastava, Prem Chandra Pandey, and Jyoti K. Sharma. An approach for route optimization in applications of precision agriculture using UAVs. *Drones*, 4(3):58, sep 2020. DOI: 10.3390/drones4030058.

[14] S.A. Bortoff. Path planning for UAVs. In *Proceedings of the 2000 American Control Conference*. IEEE, 2000. DOI: 10.1109/acc.2000.878915.

[15] Marcus Oliver Letzel, Martina Krane, and Siegfried Raasch. High resolution urban large-eddy simulation studies from street canyon to neighbourhood scale. *Atmospheric Environment*, 42(38):8770–8784, dec 2008. DOI: 10.1016/j.atmosenv.2008.08.001.

[16] Manabu Kanda, Atsushi Inagaki, Takashi Miyamoto, Micha Gryschka, and Siegfried Raasch. A new aerodynamic parametrization for real urban surfaces. *Boundary-Layer Meteorology*, 148(2):357–377, apr 2013. DOI: 10.1007/s10546-013-9818-x.

[17] Marcus Letzel, Gabriel Gaus, Siegfried Raasch, Nils Jensen, and Manabu Kanda. Turbulent flow around high-rise office buildings in downtown tokyo. dynamic visualization in science, no. 13100, 2008., 04 2014.

[18] Andreas Tack, Jarkko Koskinen, Antti Hellsten, Pauli Sievinen, Igor Esau, Jaan Praks, Jaakko Kukkonen, and Martti Hallikainen. Morphological database of paris for atmospheric modeling purposes. *IEEE Journal of Selected Topics in Applied Earth Observations and Remote Sensing*, 5(6):1803–1810, dec 2012. DOI: 10.1109/jstars.2012.2201134.

[19] Akio Arakawa and Vivian R. Lamb. Computational design of the basic dynamical processes of the UCLA general circulation model. In *Methods in Computational Physics: Advances in Research and Applications, Vol. 17*, pages 173–265. Elsevier, 1977. DOI: 10.1016/b978-0-12-460817-7.50009-4.

[20] Palmgroup. *E3: Flow around a cubical building*. Institute of Meteorology and Climatology, Leibniz Universität Hannover, 09 2020.

[21] S. Nishizawa and Y. Kitamura. A surface flux scheme based on the monin–obukhov similarity for finite volume models. *Journal of Advances in Modeling Earth Systems*, dec 2018. DOI: 10.1029/2018ms001534.

[22] N. H. McClamroch. *Steady Aircraft Flight and Performance*. Princeton University Press, Princeton, 2011. ISBN: 9781680159097.